

Stochastic Mutation Theory of SARS-CoV-2 Variants

Liaofu Luo^{1*}, Jun Lv^{2*}

¹Faculty of Physical Science and Technology, Inner Mongolia University, 235 West College Road, Hohhot 010021, PR China

²College of Science, Inner Mongolia University of Technology, 49 Aymin Street, Hohhot 010051, PR China

*Correspondence: Liaofu Luo, lolfcm@imu.edu.cn; Jun Lv, ljun@imut.edu.cn

Abstract Predicting the future evolutionary trajectory of SARS-CoV-2 remains a critical challenge, particularly due to the pivotal role of spike protein mutations. Developing an evolutionary model capable of continuously integrating new experimental data is an urgent priority. By employing well-founded assumptions for mutant representation (four-letter and two-letter formats) and the n -mer distance algorithm, we constructed an evolutionary tree of SARS-CoV-2 mutations that accurately reflects observed viral strain evolution. We introduce a stochastic method for generating new strains on this tree based on spike protein mutations. For a given set A of existing mutation sites, we define a set X of x randomly generated sites on the spike protein. Our analysis reveals that the position of a generated strain on the tree is determined by x . Through large-scale stochastic sampling, we predict the emergence of new macro-lineages. As x increases, the proportions of macro-lineages shift: lineage O surpasses lineage N, lineage P overtakes O, and ultimately, new lineage Q surpasses P. We identified threshold values of x that distinguish between macro-lineages. Furthermore, we demonstrate that the linear regression of the number of mutated sites (x) against sample collection dates (t) provides a robust approximation, enabling the prediction of new lineage emergence based on the x - t relationship. To conclude, we demonstrated that the SARS-CoV-2 evolution adheres to statistical principles: the emergence of new strains on the evolutionary tree can be driven by randomly generated spike protein sites; and the large-scale stochastic sampling uncovers evolutionary patterns governing the emergence of diverse macro-lineages.

Keywords SARS-CoV-2, spike protein mutation, evolutionary analysis

Background

Severe Acute Respiratory Syndrome Coronavirus 2 (SARS-CoV-2) has continuously mutated over the past five years, resulting in the emergence of numerous variants, including Alpha, Beta, Gamma, Delta, and Omicron. The intricate interplay among viral antigenicity, transmission

dynamics, and virulence poses significant challenges in predicting the future trajectory and disease burden of Coronavirus Disease 2019 (COVID-19) [1-6]. Recent studies have proposed innovative approaches to forecast the evolution of the pandemic. For instance, a network-based inference method has been suggested for short- to medium-term predictions, although its reliability diminishes for long-term forecasting [7]. Given the critical role of spike protein mutations in SARS-CoV-2 evolution, deep learning techniques, particularly those leveraging Large Language Models, have been developed to predict future protein sequences [8-11]. Among these, the PandoGen algorithm has demonstrated promise in training protein language models for pandemic protein forecasting [8]. Nevertheless, challenges remain in utilizing PandoGen to predict recombinant SARS-CoV-2 lineages and ensuring the continuous integration of new experimental data.

Recent research has identified two primary drivers of viral evolution: intrinsic transmissibility, determined by the angiotensin-converting enzyme 2 (ACE2) binding affinity of SARS-CoV-2, and immune evasion, achieved through reduced susceptibility to neutralizing antibodies [12]. Computational analyses of affinity dynamics have also been explored in recent literature [13]. Building on these two forces, we propose an evolutionary model for viral mutations. Our approach involves constructing an evolutionary tree based on well-founded assumptions regarding mutant representation, combined with the application of a robust tree construction algorithm. Notably, we demonstrate that the theoretical tree accurately reflects the observed evolutionary patterns of existing viral strains. Furthermore, by leveraging a statistical method developed in our study, we extend the utility of the evolutionary tree to predict the emergence of novel macro-lineages. Our findings reveal that the probability of a macro-lineage's emergence is correlated with the number of stochastically mutated sites on the spike protein. As this number increases, the proportions of macro-lineages shift: lineage O surpasses lineage N, followed by lineage P surpassing lineage O, and ultimately, lineage Q surpassing lineage P. We initially predicted the emergence of macro-lineage P, which has since been confirmed [14]. On the other hand, in a previous study [15], we developed a mathematical model to analyze the dynamics of COVID-19 spread, with a particular focus on the competitive transmission of two viral strains within a region. Importantly, the prediction of new macro-lineage emergence is closely tied to such competitive dynamics. These results provide a vital theoretical foundation for understanding the evolution of SARS-CoV-2.

Another challenge lies in the precise prediction of the timeline for SARS-CoV-2 evolution. To forecast the future trajectory of macro-lineage P and the emergence of macro-lineage Q, it is crucial to understand how the number of mutated sites on the spike protein of selected SARS-CoV-2 variants evolves over time. Despite the complexity of factors influencing viral evolution, we identified an approximately linear relationship between the number of mutated sites for a given variant and the date of its first global sample collection. This relationship allows us to predict the timeline of macro-lineage transformations with greater accuracy.

Methods

Retrieval of SARS-CoV-2 variant data

We identified 62 variants from mutation reports provided by outbreak.info (<https://outbreak.info/>, accessed on January 4, 2025) [16], all of which belong to SARS-CoV-2 Pango lineages. Our analysis focused exclusively on mutations in the viral spike protein. The number of mutated sites in the spike protein and the first global sample collection dates for each variant are listed in Table 1, arranged in chronological order. Characteristic mutations for each lineage were defined as nonsynonymous substitutions or deletions present in over 75% of sequences within that lineage. A complete list of the 62 variants and their mutation sites is provided in Table S1 (Supplementary Data).

Table 1 Collection dates of SARS-CoV-2 variants and numbers of mutated sites on spike protein

Macro-lineage	Variant	NMS *	Earliest date ‡	Variant	NMS *	Earliest date ‡
N-lineage	B.1	1	15 Jan 2020	B.1.621	9	19 Sep 2020
	B.1.177	2	7 Mar 2020	C.37	14	8 Nov 2020
	P.2	3	15 Apr 2020	B.1.526	4	15 Nov 2020
	B.1.1.7	10	14 May 2020	B.1.525	9	11 Dec 2020
	B.1.429	4	6 Jul 2020	P.3	7	15 Jan 2021
	B.1.351	10	9 Jul 2020	AZ.2	6	5 Feb 2021
	B.1.617.2	9	7 Sep 2020	AV.1	10	23 Mar 2021
	P.1	12	11 Sep 2020	B.1.1.529	7	15 Apr 2021
	B.1.617.1	5	15 Sep 2020	C.1.2	15	11 May 2021
O-lineage	BA.1	33	27 Jan 2021	BN.1.2	40	7 Feb 2022
	BA.1.1	35	28 Jan 2021	CH.1.1	41	12 May 2022
	BA.2	31	25 Mar 2021	XBB.1.5	42	12 Jun 2022
	BA.2.12.1	33	28 Sep 2021	BM.4.1.1	39	20 Jul 2022
	BA.2.65	31	11 Oct 2021	CH.1.1.1	42	15 Oct 2022
	BA.1.1.15	37	27 Nov 2021	XBB.1.16	43	4 Jan 2023
	BA.5	34	9 Dec 2021	EG.1	43	16 Jan 2023
	BA.4.1	35	14 Dec 2021	HV.1	46	29 Jan 2023
	BQ.1.1	37	20 Dec 2021	HK.3	45	29 Jan 2023
	BA.2.75	30	31 Dec 2021	EG.5.1	44	31 Jan 2023
	BF.5	35	8 Jan 2022	DV.7.1	45	29 May 2023
	BF.7	35	24 Jan 2022			
P-lineage	JN.1	60	13 Jan 2023	KP.3	63	7 Jan 2024
	BA.2.86.1	59	17 Jan 2023	LB.1	64	15 Jan 2024
	BA.2.86	58	11 Mar 2023	KP.1	63	1 Feb 2024
	JN.2	59	22 Jun 2023	KS.1	58	15 Feb 2024
	JN.1.7	62	25 Sep 2023	KP.1.1.3	65	23 Feb 2024
	JN.1.11.1	62	29 Dec 2023	XDV.1	56	26 Feb 2024
	KP.3.1.1	64	1 Jan 2024	LP.1	66	22 Apr 2024
	KP.2	59	2 Jan 2024	XED	64	19 Jun 2024
	JN.1.37	61	3 Jan 2024	XEC	65	28 Jun 2024
	XEB	61	3 Jan 2024	LF.7	67	26 Aug 2024
	XDQ.1	55	5 Jan 2024			

* NMS: number of mutated sites. ‡ Dates : the worldwide first sample collection date.

ACE2 binding affinity of single mutations and four-letter representation of mutants

We obtained data on single-point mutations affecting the interaction between the receptor-binding domain (RBD) (amino acid residues 331 to 531 of the spike protein) and the ACE2 receptor from reference [17]. For each mutation at the i -th residue, the mean and standard deviation of the binding affinity are denoted as b_i and s_i , respectively. A mutation is classified as affinity-enhancing if its affinity value (m_i) satisfies $m_i > b_i + s_i$; as affinity-weakening if $m_i < b_i - s_i$; and as having negligible effect if $b_i - s_i \leq m_i \leq b_i + s_i$.

The surface of coronaviruses is decorated with a spike protein, which consists of approximately 1273 amino acids in SARS-CoV-2. We represent each SARS-CoV-2 strain as a sequence of four letters, where each letter corresponds to a mutation type at a specific position. The four-letter code is defined as follows: 0 indicates no mutation relative to the wild type; 1 indicates a mutation with negligible effect on ACE2 binding affinity; 2 denotes an affinity-enhancing mutation; and 3 signifies an affinity-weakening mutation. Thus, the full spike protein of a SARS-CoV-2 mutant is represented by a 1273-character sequence of four letters. For regions outside the RBD, only two letters (0 and 1) are required.

Construction of the evolutionary tree

The evolutionary tree illustrates the relationships among different viral strains. Consistency with the tree of life is a critical requirement for any proposed evolutionary model, serving as a rigorous test for its validity. Let p_a represent the probability of a letter " a " (where a can be 0, 1, 2, or 3) occurring in a sequence, and let p_{ab} denote the joint probability of letters " a " and " b " appearing consecutively. In general, let $\sigma = abc\dots$ represent an n -letter segment, and p_σ the joint probability of the bases in σ occurring in the sequence. For the calculation of joint probabilities, all sequences are assumed to be circular. For any given n , the sum of the joint probabilities over all segments σ of length n always equals 1, i.e.,

$$\sum_{\sigma} p_{\sigma} = 1,$$

where the summation is over all 4^n segments of length n .

For two sequences Σ and Σ' , with corresponding joint probability sets $\{p_{\sigma}\}$ and $\{p'_{\sigma}\}$, we define the n -mer distance between the two sequences based on the difference in joint probabilities as:

$$E_n(\Sigma, \Sigma') = \sum_{\sigma} |p_{\sigma} - p'_{\sigma}|, \quad n=1,2,\dots \quad (1)$$

Here, the arguments of E_n are omitted when there is no ambiguity. The n -mer distance is well-defined for sequences of unequal lengths that are not aligned. By repeatedly applying relations such as the following:

$$|p_\sigma - p'_\sigma| = |\sum_a(p_{\sigma a} - p'_{\sigma a})| \leq \sum_a |p_{\sigma a} - p'_{\sigma a}|, \quad (2)$$

where σ is any n -letter segment and σa is an $(n+1)$ -letter segment, it follows that:

$$E_{n+1} \geq E_n, \quad n=1,2,\dots \quad (3)$$

To infer the phylogenetic tree, three main algorithms are commonly used: distance matrix treeing, maximum parsimony analysis, and the maximum likelihood method [18]. In this study, we employed the unweighted pair group method with arithmetic mean (UPGMA) [19] to construct the phylogenetic tree.

Least squares regression analysis

Least squares regression analysis was performed to examine the relationship between the number of mutated sites and the first sample collection date of the variants. For a dependent variable y and an independent variable x , with observed values y_i at $x=x_i$, the linear regression equation is given by:

$$\hat{y} = \hat{\beta}_0 + \hat{\beta}_1 x, \quad (4)$$

where \hat{y} is the predicted value, and $\hat{\beta}_0$ and $\hat{\beta}_1$ are the regression coefficients. The standard error of the prediction $SE(\hat{y})$ is calculated as:

$$SE(\hat{y}) = s \sqrt{\frac{1}{n} + \frac{(x-\bar{x})^2}{\sum_{i=1}^n (x_i-\bar{x})^2}}, \quad (5)$$

where \bar{x} is the mean of the x_i values, and n is the number of samples. The standard error of the slope $\hat{\beta}_1$ is:

$$SE(\hat{\beta}_1) = s \sqrt{\frac{1}{\sum_{i=1}^n (x_i-\bar{x})^2}}, \quad (6)$$

and the standard error of the intercept $\hat{\beta}_0$ is:

$$SE(\hat{\beta}_0) = s \sqrt{\frac{1}{n} + \frac{\bar{x}^2}{\sum_{i=1}^n (x_i-\bar{x})^2}}. \quad (7)$$

In equations (5)-(7), s represents the Residual Standard Error (RSE), also known as the model's sigma, defined as:

$$s = \sqrt{\frac{\sum_{i=1}^n (y_i - \hat{y}_i)^2}{n-2}}. \quad (8)$$

The 95% confidence interval for parameter estimates is calculated to capture the true value with 95% probability. The confidence interval is given by:

$$CI(\hat{q}) = \hat{q} \pm t(\alpha/2, df) \cdot SE(\hat{q}), \quad (9)$$

where $\hat{q} \in \{\hat{y}, \hat{\beta}_1, \hat{\beta}_0\}$, and $t(\alpha/2, df)$ is the critical value from the t-distribution with confidence level α and degrees of freedom df . For a 95% confidence interval, $\alpha=5\%$.

The model's performance is assessed using R^2 (R-squared) and the Residual Standard Error (RSE). A high R^2 (close to 1) and a low RSE indicate a good fit of the model.

Results and Discussion

Evolutionary tree of virus mutations reconstructed using the UPGMA method

Without loss of generality, we applied the n -mer distance method to construct a distance matrix D

for the 25 SARS-CoV-2 variants listed in Table S2. This matrix is based on mutants labeled i, j, k, \dots , where the element D_{ij} represents the n -mer distance between sequences Σ_i and Σ_j , with each Σ_i denoting the sequence of mutant i . By applying the UPGMA algorithm to this distance matrix, we reconstructed the evolutionary tree of the 25 mutants for a specific value of n . We observed that the cladogram structure of the tree stabilizes after several iterations as n increases, reaching stability when $n \geq 7$ [14]. Detailed comparisons of tree structures for different values of n are provided in the supplementary data. Fig. 1 shows the UPGMA tree reconstructed using $n=7$.

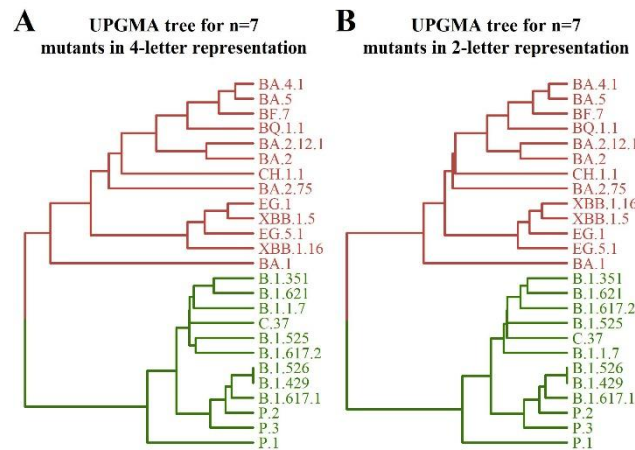


Fig. 1 Evolutionary tree describing virus mutation. (A) The mutants in 4-letter representation. (B) The mutants in 2-letter representation

In Figure 1, two prominent branches represent the macro-lineages N and O of the virus strains. Within macro-lineage O, the sub-branches clearly depict the divergence of the BA.1 strain into BA.2, BA.4, and BA.5 (The bifurcation of BA.1 from other strains of the O-lineage is consistent with the recent phylogeny by Nextstrain [20]), as well as the accurate classification of XBB as a recombination of two BA.2 strains. In macro-lineage N, the sub-branch includes four variants of concern (VOCs): B.1.1.7 (Alpha), B.1.351 (Beta), B.1.617.2 (Delta), and P.1 (Gamma), each representing independent sub-lineages. These observations confirm that the theoretical tree aligns with the evolutionary characteristics of the virus strains [6].

The only key assumption in the tree reconstruction process is the four-letter representation of mutants and the n -mer distance algorithm. This four-letter representation uses binary values (0 and 1) for 104 mutational sites on the spike protein, with additional options (2 and 3) allowed for 27 sites on the receptor-binding domain (RBD). To simplify calculations, we approximated this four-letter representation with a two-letter version, ignoring choices 2 and 3. A comparison of the two-letter and four-letter representations for the 25 mutants is shown in Fig. 1. Further comparisons for larger mutant sets (namely, 36 mutants and 62 mutants) are available in the supplementary data. We found that the cladogram structures of the tree are identical when the two-letter approximation is used.

Why does the two-letter version approximate the four-letter representation? Due to the interaction between the RBD and the human ACE-2 receptor, the 201 amino acid residues on the

RBD cannot vary independently [13]. This interaction reduces the informational content in the RBD from $\ln(4^{201})/\ln 2=402$ bits to $\ln(201 \times 20)/\ln 2=12$ bits, which constitutes a small portion of the total information in the 1273-length sequence (1273 bits). Therefore, using the two-letter approximation that omits choices 2 and 3 in the RBD is a reasonable simplification.

Generation of new strains on the evolutionary tree using a stochastic method

Once the evolutionary tree is constructed from known virus mutant lineages, new strains can be generated and examined within this framework. In this section, we present a stochastic approach to model this process. Let A represent the set of all mutated sites in the updated virus strains, with a denoting the number of these sites. Each strain is represented by a two-letter sequence derived from the set $A(a)$.

Considering stochastic mutations on the spike protein, let X be the set of x sites involved in the stochastic sampling. The union of sets $A(a)$ and $X(x)$ is denoted as Z , where $Z=A \cup X$. The intersection of sets A and X , containing y sites, is represented as $Y(y)$. Assuming the new strain arises from stochastic sampling within the set Z , the new strain is represented by a two-letter sequence from the union set $Z(\text{len})$, where $\text{len}=a+x-y$.

Since the UPGMA method effectively captures the evolutionary traits of virus mutations, we use it (with $n=7$) to reconstruct the evolutionary tree of mutants in set Z , which now includes the predicted new strain. This method is referred to as the A-X model.

Importantly, regardless of how the sets A and X are distributed along the sequence or how set Y is incorporated, the new strain can always be predicted. The model ensures accurate predictions, even with the continuous addition of new experimental data.

In the A-X model, the new strain is represented by a two-letter sequence from the union set Z . Suppose set A contains m mutants. Fig. 2A illustrates the schematic representation of the union set $Z=A \cup X$ and its relationship with sets A , X , and Y . Fig. 2B shows the coding rules for the m mutants and one new strain.

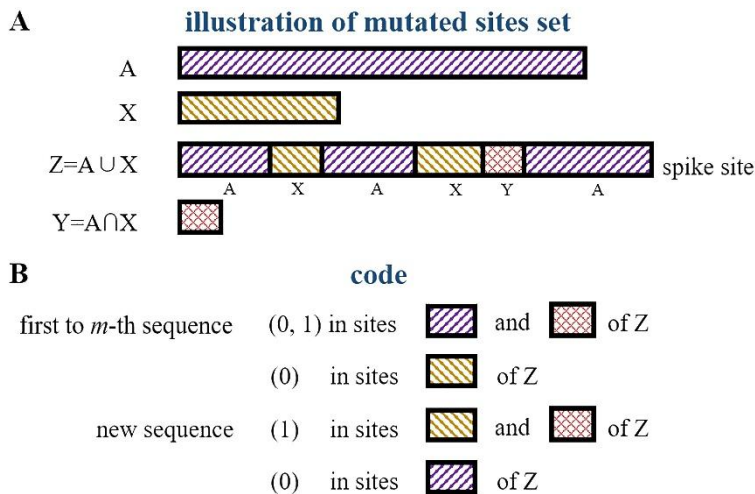


Fig. 2 Sketch map of mutated-site sets and coding rules

To demonstrate the feasibility of the A-X model in predicting new SARS-CoV-2 strains, consider the example of 25 mutants listed in Table S2. Assume the evolutionary tree of the 25 mutants in set A has two main branches, N and O. By performing stochastic sampling S times, for example $S=10^5$, we generate 10^5 predictions for new strains. We observe the following:

1. The new strain may belong to one of the two main branches, N or O, or it may fall outside both, suggesting it belongs to a new macro-lineage.
2. When x is small, the predicted new strain typically falls within one of the two main branches, N and O. However, when x exceeds a certain threshold, an anomaly occurs, indicating the emergence of a new macro-lineage, with the new strain belonging to this lineage.
3. For a given x , different values of y can lead to distinct predictions regarding the position of the new strain on the tree. The position of the new strain is determined by the pair (x, y) . Therefore, for a given pair (x, y) , the predicted new strain on the tree is denoted as $\text{New}_{x,y}$.

Expanding the scope of stochastic sampling and predicting new SARS-CoV-2 macro-lineages

The generation of new strains in a phylogenetic tree is a stochastic process. As the scale of stochastic sampling increases, statistical patterns begin to emerge. To expand the scope of stochastic sampling, we found that increasing the size of x and randomizing parameter y within the intersection set, in conjunction with the increase of x , is a viable approach. This technique effectively enhances the stochastic information, facilitating new discoveries regarding the emergence of new macro-lineages.

Generation of multiple macro-lineages

At a given time t , we can predict the emergence of new variants from set $A(a)$. In the A-X model, the selection of set X is stochastic, leading to the random appearance of new variants on the phylogenetic tree. However, the generation of multiple macro-lineages and the subsequent bifurcation of the tree topology into several major branches are inevitable.

For instance, at $t = T_1$ (October 15, 2023), we performed 10^5 rounds of stochastic sampling for x and 6 rounds of randomization for y . During this process, we consistently observed the inevitable emergence of macro-lineages N, O, and P. The probability of a lineage (N, O, or P) for a given x is calculated by dividing the occurrence count of each lineage by the total number of variants (10^5). Specifically, the macro-lineage to which a newly generated variant belongs is determined by its occurrence in the bifurcation of the phylogenetic tree. The results are illustrated in Fig. 3, where the probability of the j -lineage ($j=N, O, \text{ or } P$) is plotted against x .

The calculation uses a 99% percentile. We found that the assignment of a macro-lineage to a new variant depends statistically on x , with specific demarcation values distinguishing different macro-lineages as follows:

$\text{New}_{x,y} \in N$ when $x \leq 18$; $\text{New}_{x,y} \in N$ or O when $18 < x \leq 29$; $\text{New}_{x,y} \in O$ when $29 < x \leq 36$; $\text{New}_{x,y} \in O$ or P when $36 < x \leq 69$; and $\text{New}_{x,y} \in P$ when $x > 69$.

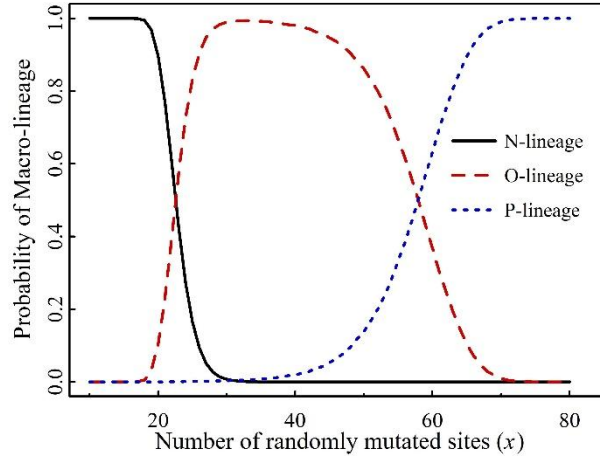


Fig. 3 PML(Probability of Macro-lineage) vs x for 25 mutants ($a=104$)

At a later time, T_2 (July 20, 2024), after incorporating 11 new mutants (listed in Table S3) into set A , the value of a increased from 104 to 128, covering a total of 36 mutants. We again performed 10^5 rounds of stochastic sampling for x and 6 rounds of randomization for y . The probabilities of the j -lineage ($j = N, O, P, \text{ or } Q$) are shown in Fig. 4.

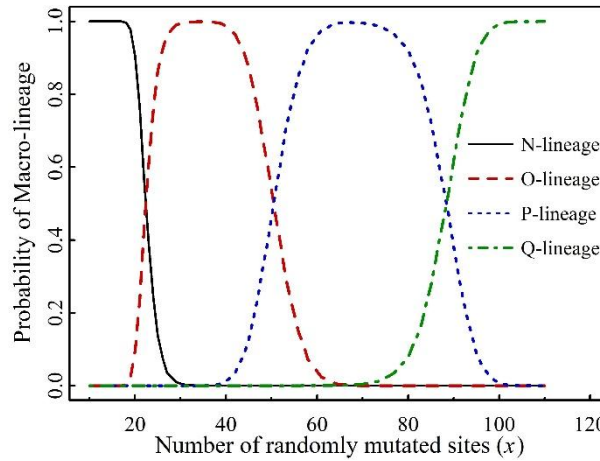


Fig. 4 PML(Probability of Macro-lineage) vs x for 36 mutants ($a=128$)

Using the same method, we obtained the following demarcation values for x in the case of 36 mutants:

$\text{New}_{x,y} \in N$ when $x \leq 18$; $\text{New}_{x,y} \in N$ or O when $18 < x \leq 29$; $\text{New}_{x,y} \in O$ when $29 < x \leq 39$; $\text{New}_{x,y} \in O$ or P when $39 < x \leq 62$; $\text{New}_{x,y} \in P$ when $62 < x \leq 72$; $\text{New}_{x,y} \in P$ or Q when $72 < x \leq 99$ and $\text{New}_{x,y} \in Q$ when $x > 99$.

At the next time point, T_3 (January 4, 2025), after incorporating 62 variants from Table S1 into set A , the value of a increased to 146. The probabilities of the j -lineage (where $j = N, O, P, \text{ or } Q$) for 62 mutants are presented in Fig. 5. The demarcation values for x are:

$\text{New}_{x,y} \in N$ when $x \leq 20$; $\text{New}_{x,y} \in N$ or O when $20 < x \leq 30$; $\text{New}_{x,y} \in O$ when $30 < x \leq 37$; $\text{New}_{x,y} \in O$ or P when $37 < x \leq 62$; $\text{New}_{x,y} \in P$ when $62 < x \leq 79$; $\text{New}_{x,y} \in P$ or Q when $79 < x \leq 108$ and $\text{New}_{x,y} \in Q$ when $x > 108$.

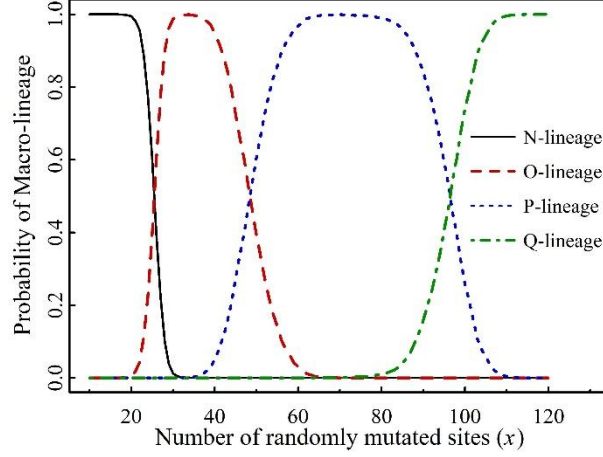


Fig. 5 PML(Probability of Macro-lineage) vs x for 62 mutants ($a=146$)

Law for the Emergence of Novel Macro-Lineages

Set $A(a)$ is an observable set that depends on time t . Set X represents the set of assumed mutated sites, also dependent on t , used to predict new macro-lineages. We define x_{dem1} as the demarcation value of x at which the occurrence of a new macro-lineage has a nonzero probability (greater than 1% in calculations), and x_{dem2} as the demarcation value for its definitive occurrence. Both x_{dem1} and x_{dem2} are functions of time t .

At time t_k , let the value of a be denoted as a_k , with examples $a_1 = 104$, $a_2 = 128$ and $a_3 = 146$. Denote x_{dem1} for macro-lineage j (where $j = O, P, Q$) at time t_k as $x_{\text{dem1}}^{(j)}(t_k)$, and similarly, denote x_{dem2} for macro-lineage j at time t_k as $x_{\text{dem2}}^{(j)}(t_k)$. The values of $x_{\text{dem1}}^{(j)}(t_k)$ and $x_{\text{dem2}}^{(j)}(t_k)$ are shown in Figs. 3, 4 and 5, and summarized in Table 2.

Table 2 Demarcation values x_{dem1} and x_{dem2} at three times t_1 and t_2 and t_3

k	a_k	$x_{\text{dem1}}^{(O)}(t_k)$	$x_{\text{dem2}}^{(O)}(t_k)$	$x_{\text{dem1}}^{(P)}(t_k)$	$x_{\text{dem2}}^{(P)}(t_k)$	$x_{\text{dem1}}^{(Q)}(t_k)$	$x_{\text{dem2}}^{(Q)}(t_k)$
1	104	19	30	37	70	-	-
2	128	19	30	40	63	73	100
3	146	21	31	38	63	80	109

Note: $t_1 < t_2 < t_3$. t_1 is the time period later than January 31, 2023 that includes T_1 =October 15, 2023, t_2 is the time period later than February 1, 2024 that includes T_2 = January 20, 2024, t_3 is the time period later than August 26, 2024 that includes T_3 = January 4, 2025. The starting point for each time period can be found in Table S2, S3 and S1 respectively.

Table 2 outlines the occurrence pattern for novel macro-lineages: the O-lineage emerges at $x \approx 19 - 21$, and definitely occurs at $x \approx 30 - 31$; the P-lineage emerges at $x \approx 37 - 40$, and definitely occurs at $x \approx 63 - 70$; the Q-lineage emerges at $x \approx 73 - 80$, and definitely occurs at $x \approx 100 - 109$. The demarcation values deduced in different time periods are highly consistent.

From Table 2 and Fig. 3, we predicted the emergence of the P-lineage at time t_1 . However, no P-lineage is observed in the phylogenetic tree for 25 mutants (Fig. 1, Fig. S1). The P-lineage appears in the phylogenetic tree for 36 or more mutants (Fig. S2). This suggests that our prediction was made earlier than the actual observation and phylogenetic analysis. Similarly, based on Table 2 we predicted the emergence of the Q-lineage at times t_2 and t_3 . Although there

are no current observations or phylogenetic analyses supporting the presence of macro-lineage Q (Fig. S2 and S3), we predict its existence based on the present data of mutants (Fig. 4 and Fig. 5).

Mutation sites increase over time in SARS-CoV-2 variants

Each macro-lineage of SARS-CoV-2 has a specific survival time. The relationship between the number of mutated sites and time t is a discontinuous function

In this study, we explore the relationship between the number of mutated sites on the spike protein of selected SARS-CoV-2 variants and the first sample collection date. To quantify this, we introduce $NMS(t)$, representing the number of mutated sites that have increased around the first sample collection date t . Our findings show that $NMS(t)$ is a discontinuous function of time, corresponding to three distinct macro-lineages, as illustrated in Fig. 6. Fig. 6 is based on the data presented in Table 1.

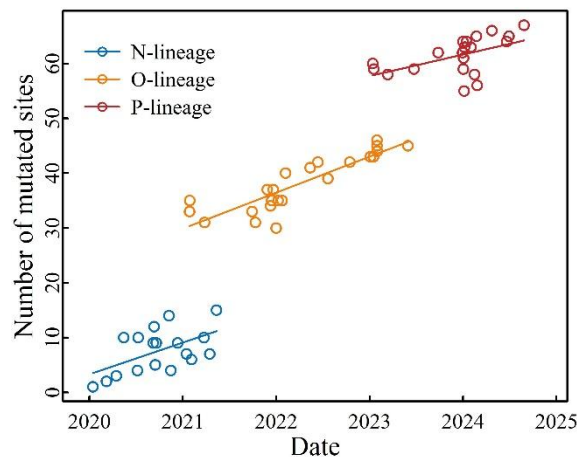


Fig. 6 Number of mutated sites as a function of the first sample collection date

Linear regression of mutated sites vs. sample collection date as an approximation

We performed linear regression to examine the relationship between the number of mutated sites and the first sample collection date, with the results presented in Fig. 7. The linear regression model effectively approximates the increasing trend in the number of mutated sites over the course of viral evolution. The R^2 and RSE for the linear regression of NMS are 0.91 and 6.48, respectively. Additionally, applying Eqs. (6) and (9), we determined the slope of the regression line equaling 1.261 per month, with a 95% confidence interval of ± 0.100 . This linear regression provides a better fit, and we will use the linear relationship between the number of mutated sites (x) and collection time (t) to predict the emergence of new viral lineages.

Why is the increase in the number of mutated sites approximately linear with respect to emergence time? Figure 6 demonstrates that the relationship between the number of mutated sites (NMS) and time (t) is discontinuous, exhibiting a stepwise change at the point of lineage

transformation. However, the slope of NMS increase between neighboring lineages varies. Generally, the new lineage exhibits a lower slope of increase compared to the older lineage, compensating for the stepwise change during lineage transformation. This explains why the relationship between NMS and emergence time is approximately linear. Our prediction for the new lineage is based on this linear relationship, which can be extended to a longer time period.

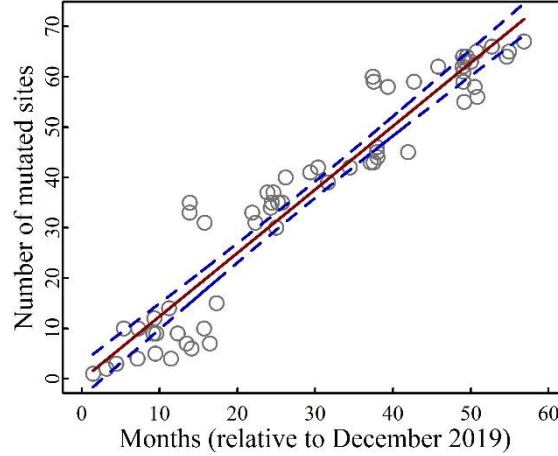


Fig. 7 Linear regression of the number of mutated sites versus the first sample collection date. The 95% confidence intervals, calculated using Eqs. (5) and (9), are represented by the blue dotted lines

Prediction of the emergence of the Q Macro-lineage

In the A-X model, the number of randomly generated sites is denoted as x for a given set A . Clearly, $NMS(t)$, which describes the increase in mutated sites over time, is intrinsically related to the number of randomly generated sites, x . Using the data from Fig. 5, which shows the probability of macro-lineage (PML) versus x , along with the time dependence of $NMS(t)$, we can predict the emergence time of the new macro-lineage Q. Based on Eqs. (4), (5), and (9), we forecast that the number of mutated sites will reach $NMS=80.4 \pm 3.8$ at the 64th month and 109 ± 6 at the 87th month, starting from December 2019. Then, combining with the demarcation values $x_{dem1} = 80$ (indicating the initial emergence of Q) and $x_{dem2} = 109$ (indicating a strong outbreak of Q), we predict that the macro-lineage Q will emerge around March 2025, and after approximately 23 months, will experience a strong outbreak.

Note: Since the emergence of Q may be masked by the high incidence of influenza during winter, the observation of its initial emergence could be delayed.

Conclusions

1. The phylogenetic tree of SARS-CoV-2 variants, reconstructed using the four-letter representation of mutants and the n -mer distance algorithm, aligns closely with experimental data

on viral evolution. Additionally, the spike protein's four-letter representation can be approximated using a two-letter representation.

2. SARS-CoV-2 evolution follows specific statistical patterns. First, the emergence of a new strain can be modeled using the A-X framework, where Set A contains existing mutated sites, and Set X consists of randomly generated sites on the spike protein. Second, by expanding the scope of stochastic sampling, we demonstrate that when the number of randomly generated sites (x) reaches a critical threshold, a new macro-lineage emerges alongside existing lineages. As x increases, the proportions of the four macro-lineages change: O surpasses N first, followed by P surpassing O, and finally, Q emerges. We also derived demarcation values of x that distinguish between different macro-lineages.

3. A linear regression between the number of mutated sites (NMS) for a variant and its global first sample collection time (t) provides an effective approximation. This linear relationship results from the combined effects of stepwise changes in NMS at lineage transitions and the varying slopes of NMS over time within neighboring lineages. The regression slope of $NMS(t)$ can be used to predict the emergence time of new macro-lineages.

List of abbreviations

SARS-CoV-2 Severe Acute Respiratory Syndrome Coronavirus 2

COVID-19 Coronavirus Disease 2019

ACE2 Angiotensin-Converting Enzyme 2

RBD Receptor-Binding Domain

UPGMA Unweighted Pair Group Method with Arithmetic Mean

RSE Residual Standard Error

PML Probability of Macro-Lineage

NMS Number of Mutated Sites

CNI Cumulative Number of Infections

Declarations

Availability of data and materials

The original data used in the study is openly available on outbreak.info at <https://outbreak.info/>.

Competing interests

The authors declare no competing interests.

Authors' contributions

Liaofu Luo: Writing – review & editing, Writing – original draft, Conceptualization, Methodology.
Jun Lv: Writing – review & editing, Methodology, Visualization, Validation. All authors reviewed the manuscript.

Acknowledgements

We sincerely appreciate Dr. Ying Zhang for her assistance with data collection, insightful discussions, and valuable suggestions.

References

1. Carabelli AM, Peacock TP, Thorne LG, Harvey WT, Hughes J, COVID-19 Genomics UK Consortium, et al. SARS-CoV-2 variant biology: immune escape, transmission and fitness. *Nat Rev Microbiol.* 2023; 21(3):162-77. <https://10.1038/s41579-022-00841-7>.
2. Markov PV, Ghafari M, Beer M, Lythgoe K, Simmonds P, Stilianakis NI, et al. The evolution of SARS-CoV-2. *Nat Rev Microbiol.* 2023; 21(6):361-79. <https://10.1038/s41579-023-00878-2>.
3. Cao Y, Jian F, Wang J, Yu Y, Song W, Yisimayi A, et al. Imprinted SARS-CoV-2 humoral immunity induces convergent Omicron RBD evolution. *Nature.* 2023; 614(7948):521-29. <https://10.1038/s41586-022-05644-7>.
4. Mallapaty S. Where did Omicron come from? Three key theories. *Nature.* 2022; 602(7895): 26-8. <https://doi.org/10.1038/d41586-022-00215-2>.
5. Callaway E. Beyond Omicron: what's next for COVID's viral evolution. *Nature.* 2021; 600(7888): 204-7. <https://doi.org/10.1038/d41586-021-03619-8>.
6. Wang Q, Iketani S, Li Z, Liu L, Guo Y, Huang Y, et al. Alarming antibody evasion properties of rising SARS-CoV-2 BQ and XBB subvariants. *Cell.* 2023; 186(2): 279-286.e8. <https://doi.org/10.1016/j.cell.2022.12.018>.
7. Rahnsch B, Taghizadeh L. Network-based uncertainty quantification for mathematical models in epidemiology. *J Theor Biol.* 2024; 577: 111671. <https://doi.org/10.1016/j.jtbi.2023.111671>.
8. Ramachandran A, Lumetta SS, Chen D. PandoGen: Generating complete instances of future SARS-CoV-2 sequences using Deep Learning. *PLoS Comput Biol.* 2024; 20(1): e1011790. <https://doi.org/10.1371/journal.pcbi.1011790>.
9. Fowler DM, Fields S. Deep mutational scanning: a new style of protein science. *Nat Methods.* 2014; 11(8): 801-7. <https://doi.org/10.1038/nmeth.3027>.
10. Elnaggar A, Heinzinger M, Dallago C, Rehawi G, Wang Y, Jones L, et al. ProtTrans: Toward understanding the language of life through self-supervised learning. *IEEE Trans Pattern Anal Mach Intell.* 2022; 44(10): 7112-27. <https://doi.org/10.1109/TPAMI.2021.3095381>.
11. Ferruz N, Schmidt S, Höcker B. ProtGPT2 is a deep unsupervised language model for protein design. *Nat*

Commun. 2022; 13(1): 4348. <https://doi.org/10.1038/s41467-022-32007-7>.

12. Ma W, Fu H, Jian F, Cao Y, Li M. Immune evasion and ACE2 binding affinity contribute to SARS-CoV-2 evolution. *Nat Ecol Evol.* 2023; 7(9): 1457-66. <https://doi.org/10.1038/s41559-023-02123-8>.

13. Sultana N, Nagesha SN, Reddy CNL, Ramesh BN, Shyamamma S, Shashidhara KS, et al. Computational analysis of affinity dynamics between the variants of SARS-CoV-2 spike protein (RBD) and human ACE-2 receptor. *Virology J.* 2024; 21(1): 88. <https://doi.org/10.1186/s12985-024-02365-3>

14. Luo L, Lv J. An evolutionary theory on virus mutation in COVID-19. *Virus Res.* 2024; 344: 199358. <https://doi.org/10.1016/j.virusres.2024.199358>.

15. Luo L, Lv J. Mathematical modelling of virus spreading in COVID-19. *Viruses.* 2023; 15(9): 1788. <https://doi.org/10.3390/v15091788>.

16. Gangavarapu K, Latif AA, Mullen JL, Alkuzweny M, Hufbauer E, Tsueng G, et al. Outbreak.info genomic reports: scalable and dynamic surveillance of SARS-CoV-2 variants and mutations. *Nat Methods.* 2023; 20(4): 512-22. <https://doi.org/10.1038/s41592-023-01769-3>.

17. Starr TN, Greaney AJ, Hilton SK, Ellis D, Crawford KHD, Dingens AS, et al. Deep mutational scanning of SARS-CoV-2 receptor binding domain reveals constraints on folding and ACE2 binding. *Cell.* 2020; 182(5): 1295-1310.e20. <https://doi.org/10.1016/j.cell.2020.08.012>.

18. Li W-H. *Molecular evolution*. Sunderland, MA: Sinauer Associates; 1997.

19. Nei M, Kumar S. *Molecular evolution and phylogenetics*. Oxford: Oxford University Press; 2000.

20. Hadfield J, Megill C, Bell SM, Huddleston J, Potter B, Callender C, et al. Nextstrain: real-time tracking of pathogen evolution. *Bioinformatics.* 2018; 34(23): 4121-23. doi: 10.1093/bioinformatics/bty407.

Supplementary Material:

Table S1 General table of 62 variants and their mutation sites

A total of 62 variants from the mutation reports provided by outbreak.info (<https://outbreak.info/>, accessed on 4 Jan 2025)

macro-lineage	No.	variant	NMS	mutated sites
N-lineage	1	B.1	1	614
	2	B.1.177	2	222,614
	3	P.2(Zeta)	3	484,614,1176
	4	B.1.1.7(Alpha)	10	69,70,144, 501,570,614,681,716,982,1118
	5	B.1.429(Epsilon)	4	13,152, 452,614
	6	B.1.351(Beta)	10	80,215,241,242,243, 417,484,501,614,701
	7	B.1.617.2(Delta)	9	19,156,157,158, 452,478,614,681,950
	8	P.1(Gamma)	12	18,20,26,138,190, 417,484,501,614,655,1027,1176
	9	B.1.617.1(Kappa)	5	452,484,614,681,1071
	10	B.1.621(Mu)	9	95,144,145, 346,484,501,614,681,950
	11	C.37(Lambda)	14	75,76,246,247,248,249,250,251,252,253, 452,490,614,859
	12	B.1.526(Iota)	4	5,95,253,614
	13	B.1.525(Eta)	9	52,67,69,70,144, 484,614,677,888
	14	P.3(Theta)	7	484,501,614,681,1092,1101,1176
	15	AZ.2	6	95,144, 484,614,681,796
	16	AV.1	10	80,95,142,144, 439,484,614,681,1130,1139
	17	B.1.1.529	7	373,478,614,655,679,681,954
	18	C.1.2	15	9,136,144,190,215,243,244, 449,484,501,614,655,679,716,859
O-lineage	19	BA.1	33	67,69,70,95,142,143,144,145,211,212, 339,371,373,375,477,478,484,493,496,498,501,505,547,614,655,679,681,764,796,856,954,969,981
	20	BA.1.1	35	67,69,70,95,142,143,144,145,211,212, 339,346,371,373,375,446,477,478,484,493,496,498,501,505,547,614,655,679,681,764,796,856,954,969,981
	21	BA.2	31	19,24,25,26,27,142,213, 339,371,373,375,376,405,408,417,440,477,478,484,493,498,501,505,614,655,679,681,764,796,954,969
	22	BA.2.12.1	33	19,24,25,26,27,142,213, 339,371,373,375,376,405,408,417,440,452,477,478,484,493,498,501,505,614,655,679,681,704,764,796,954,969
	23	BA.2.65	31	19,24,25,26,27,142,213, 339,371,373,375,376,405,408,417,440,477,478,484,493,498,501,505,614,655,679,681,764,796,954,969
	24	BA.1.1.15	37	67,69,70,95,142,143,144,145,211,212, 339,346,371,373,375,417,440,446,477,478,484,493,496,498,501,505,547,614,655,679,681,764,796,856,954,969,981
	25	BA.5	34	19,24,25,26,27,69,70,142,213, 339,371,373,375,376,405,408,417,440,452,477,478,484,486,498,501,505,614,655,679,681,764,796,954,969
	26	BA.4.1	35	3,19,24,25,26,27,69,70,142,213, 339,371,373,375,376,405,408,417,440,452,477,478,484,486,498,501,505,614,655,679,681,764,796,954,969
	27	BQ.1.1	37	19,24,25,26,27,69,70,142,213, 339,346,371,373,375,376,405,408,417,440,444,452,460,477,478,484,486,498,501,505,614,655,679,681,764,796,954,969
	28	BA.2.75	30	19,24,210,213,257, 339,371,373,375,376,405,408,417,440,446,460,477,478,484,498,501,505,614,655,679,681,764,796,954,969
	29	BF.5	35	19,24,25,26,27,69,70,142,213, 339,371,373,375,376,405,408,417,440,452,477,478,484,486,498,501,505,614,655,679,681,764,796,954,969,1020
	30	BF.7	35	19,24,25,26,27,69,70,142,213, 339,346,371,373,375,376,405,408,417,440,452,477,478,484,486,498,501,505,614,655,679,681,764,796,954,969
	31	BN.1.2	40	19,24,25,26,27,142,147,152,157,210,213,257, 339,346,356,371,373,375,376,405,408,417,440,446,460,477,478,484,490,498,501,505,614,655,679,681,764,796,954,969
	32	CH.1.1	41	19,24,25,26,27,142,147,152,157,210,213,257, 339,346,371,373,375,376,405,408,417,440,444,446,452,460,477,478,484,486,498,501,505,614,655,679,681,764,796,954,969

	33	XBB.1.5	42	19,24,25,26,27,83,142,144,146,183,213,252,339,346,368,371,373,375,376,405,408,417,440,445,446,460,477,478,484,486,490,498,501,505,614,655,679,681,764,796,954,969
	34	BM.4.1.1	39	19,24,25,26,27,142,147,152,157,210,213,257,339,346,371,373,375,376,405,408,417,440,446,460,477,478,484,486,498,501,505,614,655,679,681,764,796,954,969
	35	CH.1.1.1	42	19,24,25,26,27,142,147,152,157,185,210,213,257,339,346,371,373,375,376,405,408,417,440,444,446,452,460,477,478,484,486,498,501,505,614,655,679,681,764,796,954,969
	36	XBB.1.16	43	19,24,25,26,27,83,142,144,146,180,183,213,252,339,346,368,371,373,375,376,405,408,417,440,445,446,460,477,478,484,486,490,498,501,505,614,655,679,681,764,796,954,969
	37	EG.1	43	19,24,25,26,27,83,142,144,146,183,213,252,339,346,368,371,373,375,376,405,408,417,440,445,446,460,477,478,484,486,490,498,501,505,613,614,655,679,681,764,796,954,969
	38	HV.1	46	19,24,25,26,27,52,83,142,144,146,157,183,213,252,339,346,368,371,373,375,376,405,408,417,440,445,446,452,456,460,477,478,484,486,490,498,501,505,614,655,679,681,764,796,954,969
	39	HK.3	45	19,24,25,26,27,52,83,142,144,146,183,213,252,339,346,368,371,373,375,376,405,408,417,440,445,446,455,456,460,477,478,484,486,490,498,501,505,614,655,679,681,764,796,954,969
	40	EG.5.1	44	19,24,25,26,27,52,83,142,144,146,183,213,252,339,346,368,371,373,375,376,405,408,417,440,445,446,456,460,477,478,484,486,490,498,501,505,614,655,679,681,764,796,954,969
	41	DV.7.1	45	19,24,25,26,27,142,147,152,157,185,210,213,257,339,346,371,373,375,376,405,408,417,440,444,446,452,455,456,460,477,478,484,486,498,501,505,614,655,679,681,764,796,858,954,969
P-lineage	42	JN.1	60	19,21,24,25,26,27,50,69,70,127,142,144,157,158,211,212,213,216,245,264,332,339,356,371,373,375,376,403,405,408,417,440,445,446,450,452,455,460,477,478,481,483,484,486,498,501,505,554,570,614,621,655,679,681,764,796,939,954,969,1143
	43	BA.2.86.1	59	19,21,24,25,26,27,50,69,70,127,142,144,157,158,211,212,213,216,245,264,332,339,356,371,373,375,376,403,405,408,417,440,445,446,450,452,460,477,478,481,483,484,486,498,501,505,554,570,614,621,655,679,681,764,796,939,954,969,1143
	44	BA.2.86	58	19,21,24,25,26,27,50,69,70,127,142,144,157,158,211,212,213,216,245,264,332,339,356,371,373,375,376,403,405,408,417,440,445,446,450,452,460,477,478,481,484,486,498,501,505,554,570,614,621,655,679,681,764,796,939,954,969,1143
	45	JN.2	59	19,21,24,25,26,27,50,69,70,127,142,144,157,158,211,212,213,216,245,264,332,339,356,371,373,375,376,403,405,408,417,440,445,446,450,452,460,477,478,481,483,484,486,498,501,505,554,570,614,621,655,679,681,764,796,939,954,969,1143
	46	JN.1.7	62	19,21,24,25,26,27,50,69,70,127,142,144,157,158,211,212,213,216,245,264,332,339,356,371,373,375,376,403,405,408,417,440,445,446,450,452,455,460,477,478,481,483,484,486,498,501,505,554,570,572,614,621,655,679,681,764,796,939,954,969,1143,1150
	47	JN.1.11.1	62	19,21,24,25,26,27,50,69,70,127,142,144,157,158,211,212,213,216,245,264,332,339,356,371,373,375,376,403,405,408,417,440,445,446,450,452,455,456,460,477,478,481,483,484,486,498,501,505,554,570,614,621,655,679,681,764,796,939,954,969,1104,1143
	48	KP.3.1.1	64	19,21,24,25,26,27,31,50,69,70,127,142,144,157,158,211,212,213,216,245,264,332,339,356,371,373,375,376,403,405,408,417,440,445,446,450,452,455,456,460,477,478,481,483,484,486,493,498,501,505,554,570,614,621,655,679,681,764,796,939,954,969,1104,1143
	49	KP.2	59	19,21,50,69,70,127,142,144,157,158,211,212,213,216,245,264,332,339,346,356,371,373,375,376,403,405,408,417,440,445,446,450,452,455,456,460,477,478,481,483,484,486,498,501,505,554,570,614,621,655,679,681,764,796,939,954,969,1104,1143
	50	JN.1.37	61	19,21,24,25,26,27,50,69,70,127,142,144,157,158,211,212,213,216,245,264,332,339,356,371,373,375,376,403,405,408,417,440,445,446,450,452,455,460,477,478,481,483,484,486,498,501,505,554,570,614,621,655,679,680,681,764,796,939,954,969,1143
	51	XEB	61	19,21,24,25,26,27,50,69,70,127,142,144,157,158,211,212,213,216,245,264,332,339,356,371,373,375,376,403,405,408,417,440,445,446,450,452,455,460,477,478,481,483,484,486,498,501,505,554,570,614,621,655,679,681,7

			64,796,939,954,969,1143,1174
52	XDQ.1	55	19,21,24,25,26,27,50,69,70,127,142,144,157,158,211,212,213,216,245,264, 332,339,356,371,373,375,376,403,405,408,417,440,445,446,450,452,460, 475,483,484,486,498,501,505,554,570,614,621,655,679,681,764,796,954,9 69
53	KP.3	63	19,21,24,25,26,27,50,69,70,127,142,144,157,158,211,212,213,216,245,264, 332,339,356,371,373,375,376,403,405,408,417,440,445,446,450,452,455, 456,460,477,478,481,483,484,486,493,498,501,505,554,570,614,621,655,6 79,681,764,796,939,954,969,1104,1143
54	LB.1	64	19,21,24,25,26,27,31,50,69,70,127,142,144,157,158,183,211,212,213,216, 245,264, 332,339,346,356,371,373,375,376,403,405,408,417,440,445,446,4 50,452,455,456,460,477,478,481,483,484,486,498,501,505,554,570,614,62 1,655,679,681,764,796,939,954,969,1143
55	KP.1	63	19,21,24,25,26,27,50,69,70,127,142,144,157,158,211,212,213,216,245,264, 332,339,356,371,373,375,376,403,405,408,417,440,445,446,450,452,455, 456,460,477,478,481,483,484,486,498,501,505,554,570,614,621,655,679,6 81,764,796,939,954,969,1086,1104,1143
56	KS.1	58	50,59,69,70,127,142,144,157,158,211,212,213,216,245,264, 332,339,346,3 56,371,373,375,376,403,405,408,417,440,445,446,450,452,455,456,460,47 7,478,481,483,484,486,498,501,505,554,570,614,621,655,679,681,764,796 ,939,954,969,1087,1143
57	KP.1.1.3	65	19,21,24,25,26,27,31,50,69,70,127,142,144,157,158,211,212,213,216,245, 264, 332,339,346,356,371,373,375,376,403,405,408,417,440,445,446,450,4 52,455,456,460,477,478,481,483,484,486,498,501,505,554,570,614,621,65 5,679,681,764,796,939,954,969,1086,1104,1143
58	XDV.1	56	19,21,50,69,70,127,142,144,157,158,211,212,213,216,245,264, 332,339,35 6,371,373,375,376,403,405,408,417,440,445,446,450,452,455,456,460,477 ,478,481,484,486,498,501,505,554,570,614,621,655,679,681,764,796,939, 954,969,1143
59	LP.1	66	19,21,24,25,26,27,31,50,69,70,127,142,144,157,158,211,212,213,216,245, 264, 332,339,346,356,371,373,375,376,403,405,408,417,440,445,446,450,4 52,455,456,460,477,478,481,483,484,486,498,501,505,554,570,614,621,65 5,679,681,764,796,939,954,969,1086,1104,1143,1229
60	XED	64	19,21,24,25,26,27,31,50,69,70,127,142,144,157,158,211,212,213,216,245, 264, 332,339,346,356,371,373,375,376,403,405,408,417,440,445,446,450,4 52,455,456,460,477,478,481,483,484,486,498,501,505,554,570,614,621,65 5,679,681,764,796,939,954,969,1143,1263
61	XEC	65	19,21,22,24,25,26,27,50,59,69,70,127,142,144,157,158,211,212,213,216,2 45,264, 332,339,356,371,373,375,376,403,405,408,417,440,445,446,450,45 2,455,456,460,477,478,481,483,484,486,493,498,501,505,554,570,614,621 ,655,679,681,764,796,939,954,969,1104,1143
62	LF.7	67	19,21,22,24,25,26,27,31,50,69,70,127,142,144,157,158,182,190,211,212,2 13,216,245,264, 332,339,346,356,371,373,375,376,403,405,408,417,440,44 4,445,446,450,452,455,456,460,477,478,481,483,484,486,498,501,505,554 ,570,614,621,655,679,681,764,796,939,954,969,1143
total		146	3,5,9,13,18,19,20,21,22,24,25,26,27,31,50,52,59,67,69,70,75,76,80,83,95,1 27,136,138,142,143,144,145,146,147,152,156,157,158,180,182,183,185,19 0,210,211,212,213,215,216,222,241,242,243,244,245,246,247,248,249,250 ,251,252,253,257,264, 332,339,346,356,368,371,373,375,376,403,405,408, 417,439,440,444,445,446,449,450,452,455,456,460,475,477,478,481,483,4 84,486,490,493,496,498,501,505,547,554,570,572,613,614,621,655,677,67 9,680,681,701,704,716,764,796,856,858,859,888,939,950,954,969,981,982 ,1020,1027,1071,1086,1087,1092,1101,1104,1118,1130,1139,1143,1150,11 74,1176,1229,1263

NMS: number of mutated sites; Mutated sites are considered when they occur in at least 75% of the SARS-CoV-2 lineage sequences. Mutations in the spike protein's receptor-binding domain (RBD) are indicated in bold.

Table S2 Partial table of 25 variants and their mutation sitesA total of 25 variants from the mutation reports provided by outbreak.info (<https://outbreak.info/>, accessed on 15 October 2023)

macro-lineage	No.	variant	NMS	mutated sites
N-lineage e	1	P.2(Zeta)	3	484,614,1176
	2	B.1.1.7(Alpha)	10	69,70,144, 501,570,614,681,716,982,1118
	3	B.1.429(Epsilon)	4	13,152, 452,614
	4	B.1.351(Beta)	10	80,215,241,242,243, 417,484,501,614,701
	5	B.1.617.2(Delta)	9	19,156,157,158, 452,478,614,681,950
	6	P.1(Gamma)	12	18,20,26,138,190, 417,484,501,614,655,1027,1176
	7	B.1.617.1(Kappa)	5	452,484,614,681,1071
	8	B.1.621(Mu)	9	95,144,145, 346,484,501,614,681,950
	9	C.37(Lambda)	14	75,76,246,247,248,249,250,251,252,253, 452,490,614,859
	10	B.1.526(Iota)	4	5,95,253,614
	11	B.1.525(Eta)	9	52,67,69,70,144, 484,614,677,888
	12	P.3(Theta)	7	484,501,614,681,1092,1101,1176
O-lineage e	13	BA.1	33	67,69,70,95,142,143,144,145,211,212, 339,371,373,375,477,478,484,493,496,498,501,505,547,614,655,679,681,764,796,856,954,969,981
	14	BA.2	31	19,24,25,26,27,142,213, 339,371,373,375,376,405,408,417,440,477,478,484,493,498,501,505,614,655,679,681,764,796,954,969
	15	BA.2.12.1	33	19,24,25,26,27,142,213, 339,371,373,375,376,405,408,417,440,452,477,478,484,493,498,501,505,614,655,679,681,704,764,796,954,969
	16	BA.5	34	19,24,25,26,27,69,70,142,213, 339,371,373,375,376,405,408,417,440,452,477,478,484,486,498,501,505,614,655,679,681,764,796,954,969
	17	BA.4.1	35	3,19,24,25,26,27,69,70,142,213, 339,371,373,375,376,405,408,417,440,452,477,478,484,486,498,501,505,614,655,679,681,764,796,954,969
	18	BQ.1.1	37	19,24,25,26,27,69,70,142,213, 339,346,371,373,375,376,405,408,417,440,444,452,460,477,478,484,486,498,501,505,614,655,679,681,764,796,954,969
	19	BA.2.75	30	19,24,210,213,257, 339,371,373,375,376,405,408,417,440,446,460,477,478,484,498,501,505,614,655,679,681,764,796,954,969
	20	BF.7	35	19,24,25,26,27,69,70,142,213, 339,346,371,373,375,376,405,408,417,440,452,477,478,484,486,498,501,505,614,655,679,681,764,796,954,969
	21	CH.1.1	41	19,24,25,26,27,142,147,152,157,210,213,257, 339,346,371,373,375,376,405,408,417,440,444,446,452,460,477,478,484,486,498,501,505,614,655,679,681,764,796,954,969
	22	XBB.1.5	42	19,24,25,26,27,83,142,144,146,183,213,252, 339,346,368,371,373,375,376,405,408,417,440,445,446,460,477,478,484,486,490,498,501,505,614,655,679,681,764,796,954,969
	23	XBB.1.16	43	19,24,25,26,27,83,142,144,146,180,183,213,252, 339,346,368,371,373,375,376,405,408,417,440,445,446,460,477,478,484,486,490,498,501,505,614,655,679,681,764,796,954,969
	24	EG.1	43	19,24,25,26,27,83,142,144,146,183,213,252, 339,346,368,371,373,375,376,405,408,417,440,445,446,460,477,478,484,486,490,498,501,505,613,614,655,679,681,764,796,954,969
	25	EG.5.1	44	19,24,25,26,27,52,83,142,144,146,183,213,252, 339,346,368,371,373,375,376,405,408,417,440,445,446,456,460,477,478,484,486,490,498,501,505,614,655,679,681,764,796,954,969
total		104	3, 5, 13, 18, 19, 20, 24, 25, 26, 27, 52, 67, 69, 70, 75, 76, 80, 83, 95, 138, 142, 143, 144, 145, 146, 147, 152, 156, 157, 158, 180, 183, 190, 210, 211, 212, 213, 215, 241, 242, 243, 246, 247, 248, 249, 250, 251, 252, 253, 257, 339, 346, 368, 371, 373, 375, 376, 405, 408, 417, 440, 444, 445, 446, 452, 456, 460, 477, 478, 484, 486, 490, 493, 496, 498, 501, 505, 547, 570, 613, 614, 655, 677, 679, 681, 701, 704, 716, 764, 796, 856, 859, 888, 950, 954, 969, 981, 982, 1027, 1071, 1092, 1101, 1118, 1176	

NMS: number of mutated sites; Mutated sites are considered when they occur in at least 75% of the SARS-CoV-2 lineage sequences. Mutations in the spike protein's receptor-binding domain (RBD) are indicated in bold.

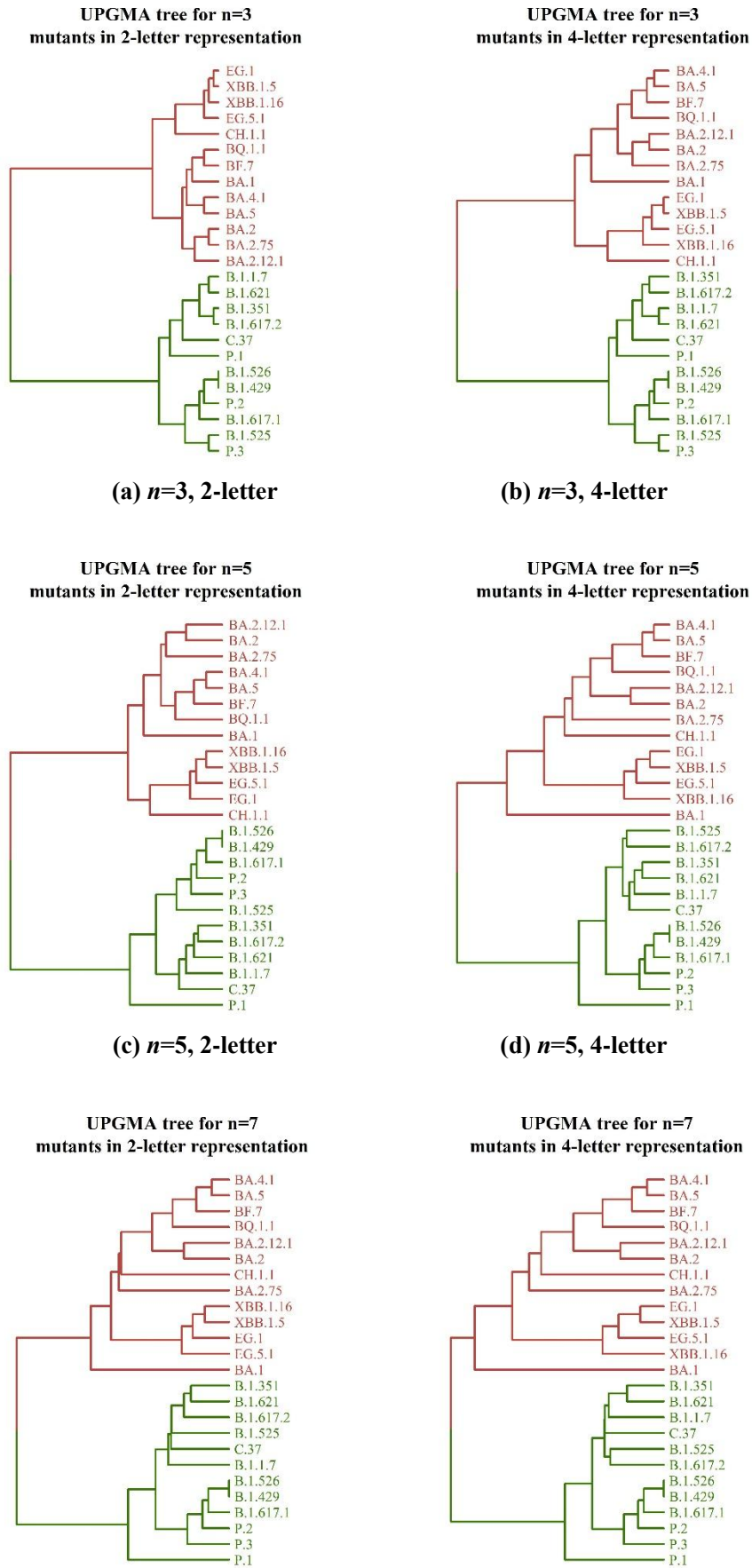
Table S3 Partial table of 36 variants and their mutation sitesA total of 36 variants from the mutation reports provided by outbreak.info (<https://outbreak.info/>, accessed on 20 July 2024)

macro-lineage	No.	variant	NMS	mutated sites
N-lineage e	1	P.2(Zeta)	3	484,614,1176
	2	B.1.1.7(Alpha)	10	69,70,144, 501,570,614,681,716,982,1118
	3	B.1.429(Epsilon)	4	13,152, 452,614
	4	B.1.351(Beta)	10	80,215,241,242,243, 417,484,501,614,701
	5	B.1.617.2(Delta)	9	19,156,157,158, 452,478,614,681,950
	6	P.1(Gamma)	12	18,20,26,138,190, 417,484,501,614,655,1027,1176
	7	B.1.617.1(Kappa)	5	452,484,614,681,1071
	8	B.1.621(Mu)	9	95,144,145, 346,484,501,614,681,950
	9	C.37(Lambda)	14	75,76,246,247,248,249,250,251,252,253, 452,490,614,859
	10	B.1.526(Iota)	4	5,95,253,614
	11	B.1.525(Eta)	9	52,67,69,70,144, 484,614,677,888
	12	P.3(Theta)	7	484,501,614,681,1092,1101,1176
O-lineage e	13	BA.1	33	67,69,70,95,142,143,144,145,211,212, 339,371,373,375,477,478,484,493,496,498,501,505,547,614,655,679,681,764,796,856,954,969,981
	14	BA.2	31	19,24,25,26,27,142,213, 339,371,373,375,376,405,408,417,440,477,478,484,493,498,501,505,614,655,679,681,764,796,954,969
	15	BA.2.12.1	33	19,24,25,26,27,142,213, 339,371,373,375,376,405,408,417,440,452,477,478,484,493,498,501,505,614,655,679,681,704,764,796,954,969
	16	BA.5	34	19,24,25,26,27,69,70,142,213, 339,371,373,375,376,405,408,417,440,452,477,478,484,486,498,501,505,614,655,679,681,764,796,954,969
	17	BA.4.1	35	3,19,24,25,26,27,69,70,142,213, 339,371,373,375,376,405,408,417,440,452,477,478,484,486,498,501,505,614,655,679,681,764,796,954,969
	18	BQ.1.1	37	19,24,25,26,27,69,70,142,213, 339,346,371,373,375,376,405,408,417,440,444,452,460,477,478,484,486,498,501,505,614,655,679,681,764,796,954,969
	19	BA.2.75	30	19,24,210,213,257, 339,371,373,375,376,405,408,417,440,446,460,477,478,484,498,501,505,614,655,679,681,764,796,954,969
	20	BF.7	35	19,24,25,26,27,69,70,142,213, 339,346,371,373,375,376,405,408,417,440,452,477,478,484,486,498,501,505,614,655,679,681,764,796,954,969
	21	CH.1.1	41	19,24,25,26,27,142,147,152,157,210,213,257, 339,346,371,373,375,376,405,408,417,440,444,446,452,460,477,478,484,486,498,501,505,614,655,679,681,764,796,954,969
	22	XBB.1.5	42	19,24,25,26,27,83,142,144,146,183,213,252, 339,346,368,371,373,375,376,405,408,417,440,445,446,460,477,478,484,486,490,498,501,505,614,655,679,681,764,796,954,969
	23	XBB.1.16	43	19,24,25,26,27,83,142,144,146,180,183,213,252, 339,346,368,371,373,375,376,405,408,417,440,445,446,460,477,478,484,486,490,498,501,505,614,655,679,681,764,796,954,969
	24	EG.1	43	19,24,25,26,27,83,142,144,146,183,213,252, 339,346,368,371,373,375,376,405,408,417,440,445,446,460,477,478,484,486,490,498,501,505,613,614,655,679,681,764,796,954,969
	25	EG.5.1	44	19,24,25,26,27,52,83,142,144,146,183,213,252, 339,346,368,371,373,375,376,405,408,417,440,445,446,456,460,477,478,484,486,490,498,501,505,614,655,679,681,764,796,954,969
26	HV.1	46	19,24,25,26,27,52,83,142,144,146,157,183,213,252, 339,346,368,371,373,375,376,405,408,417,440,445,446,452,456,460,477,478,484,486,490,498,501,505,614,655,679,681,764,796,954,969	
P-lineage	27	JN.1	60	19,21,24,25,26,27,50,69,70,127,142,144,157,158,211,212,213,216,245,264, 332,339,356,371,373,375,376,403,405,408,417,440,445,446,450,452,455,460,477,478,481,483,484,486,498,501,505,554,570,614,621,655,679,681,764,796,939,954,969,1143
	28	BA.2.86.1	59	19,21,24,25,26,27,50,69,70,127,142,144,157,158,211,212,213,216,245,264, 332,339,356,371,373,375,376,403,405,408,417,440,445,446,450,452,460,477,478,481,483,484,486,498,501,505,554,570,614,621,655,679,681,764,796,939,954,969,1143

29	BA.2.86	58	19,21,24,25,26,27,50,69,70,127,142,144,157,158,211,212,213,216,245,264, .332,339,356,371,373,375,376,403,405,408,417,440,445,446,450,452,460, 477,478,481,484,486,498,501,505,554,570,614,621,655,679,681,764,796,9 39,954,969,1143
30	JN.1.7	62	19,21,24,25,26,27,50,69,70,127,142,144,157,158,211,212,213,216,245,264, .332,339,356,371,373,375,376,403,405,408,417,440,445,446,450,452,455, 460,477,478,481,483,484,486,498,501,505,554,570,572,614,621,655,679,6 81,764,796,939,954,969,1143,1150
31	KP.3.1.1	64	19,21,24,25,26,27,31,50,69,70,127,142,144,157,158,211,212,213,216,245, 264,332,339,356,371,373,375,376,403,405,408,417,440,445,446,450,452,4 55,456,460,477,478,481,483,484,486,493,498,501,505,554,570,614,621,65 5,679,681,764,796,939,954,969,1104,1143
32	KP.2	59	19,21,50,69,70,127,142,144,157,158,211,212,213,216,245,264, 332,339,34 6,356,371,373,375,376,403,405,408,417,440,445,446,450,452,455,456,460 ,477,478,481,483,484,486,498,501,505,554,570,614,621,655,679,681,764, 796,939,954,969,1104,1143
33	JN.1.37	61	19,21,24,25,26,27,50,69,70,127,142,144,157,158,211,212,213,216,245,264 ,332,339,356,371,373,375,376,403,405,408,417,440,445,446,450,452,455, 460,477,478,481,483,484,486,498,501,505,554,570,614,621,655,679,680,6 81,764,796,939,954,969,1143
34	XDQ.1	55	19,21,24,25,26,27,50,69,70,127,142,144,157,158,211,212,213,216,245,264 ,332,339,356,371,373,375,376,403,405,408,417,440,445,446,450,452,460, 475,483,484,486,498,501,505,554,570,614,621,655,679,681,764,796,954,9 69
35	LB.1	64	19,21,24,25,26,27,31,50,69,70,127,142,144,157,158,183,211,212,213,216, 245,264,332,339,346,356,371,373,375,376,403,405,408,417,440,445,446,4 50,452,455,456,460,477,478,481,483,484,486,498,501,505,554,570,614,62 1,655,679,681,764,796,939,954,969,1143
36	KP.1	63	19,21,24,25,26,27,50,69,70,127,142,144,157,158,211,212,213,216,245,264 ,332,339,356,371,373,375,376,403,405,408,417,440,445,446,450,452,455, 456,460,477,478,481,483,484,486,498,501,505,554,570,614,621,655,679,6 81,764,796,939,954,969,1086,1104,1143
total		128	3,5,13,18,19,20,21,24,25,26,27,31,50,52,67,69,70,75,76,80,83,95,127,138, 142,143,144,145,146,147,152,156,157,158,180,183,190,210,211,212,213,2 15,216,241,242,243,245,246,247,248,249,250,251,252,253,257,264, 332,33 9,346,356,368,371,373,375,376,403,405,408,417,440,444,445,446,450,452 ,455,456,460,475,477,478,481,483,484,486,490,493,496,498,501,505,547, 554,570,572,613,614,621,655,677,679,680,681,701,704,716,764,796,856,8 59,888,939,950,954,969,981,982,1027,1071,1086,1092,1101,1104,1118,11 43,1150,1176

NMS: number of mutated sites; Mutated sites are considered when they occur in at least 75% of the SARS-CoV-2 lineage sequences. Mutations in the spike protein's receptor-binding domain (RBD) are indicated in bold.

Figure S1 Phylogenetic tree of 25 mutants (total number of mutated sites =104)

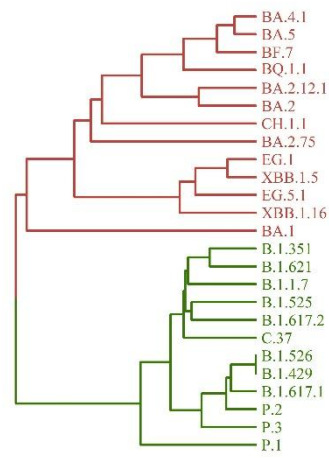
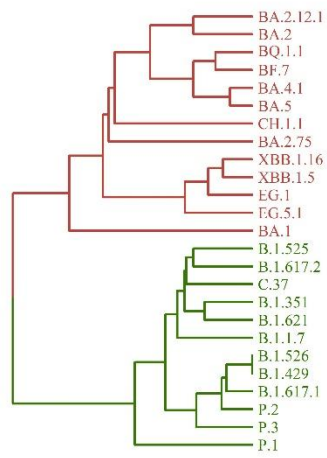


(e) $n=7$, 2-letter

(f) $n=7$, 4-letter

**UPGMA tree for $n=8$
mutants in 2-letter representation**

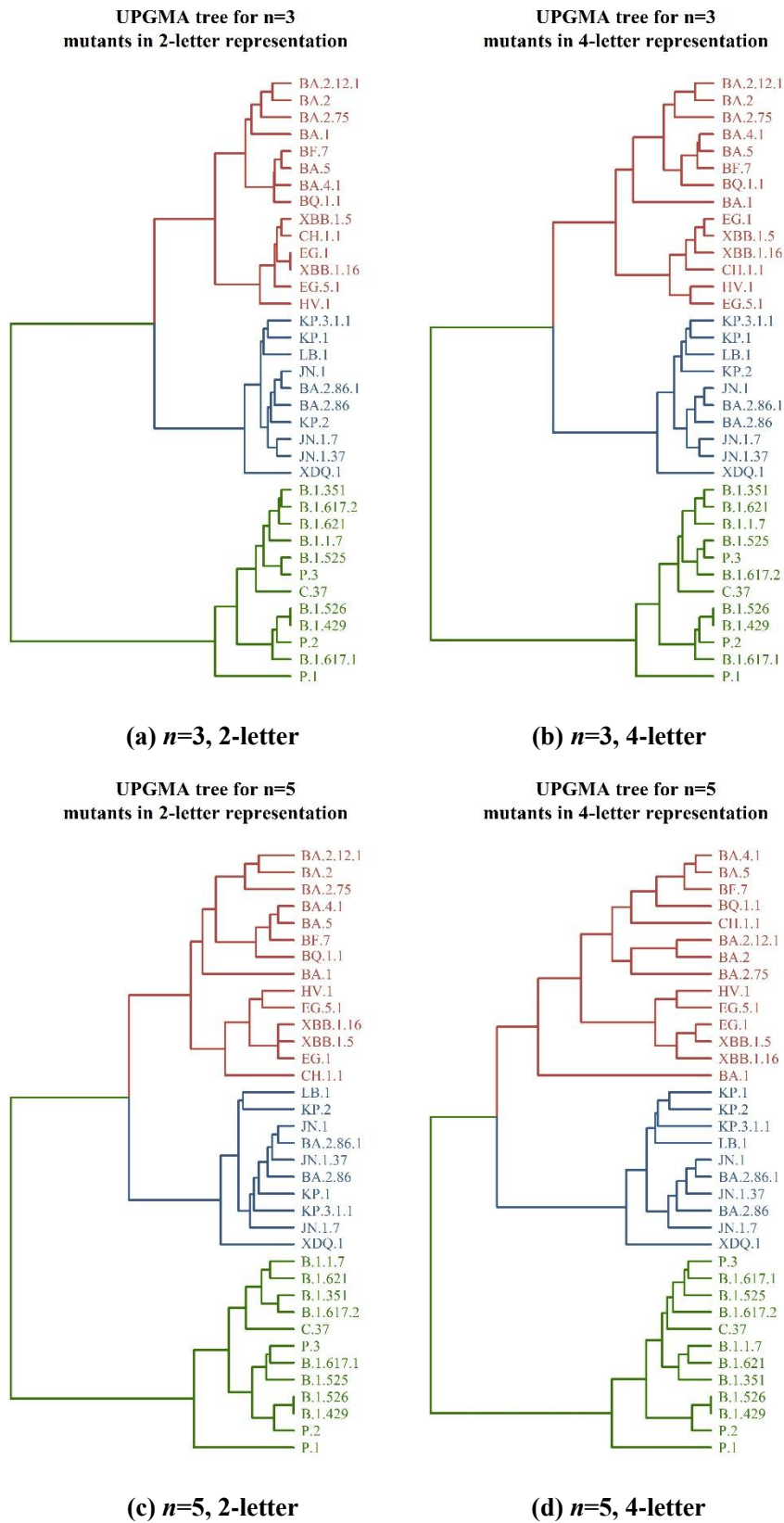
**UPGMA tree for $n=8$
mutants in 4-letter representation**



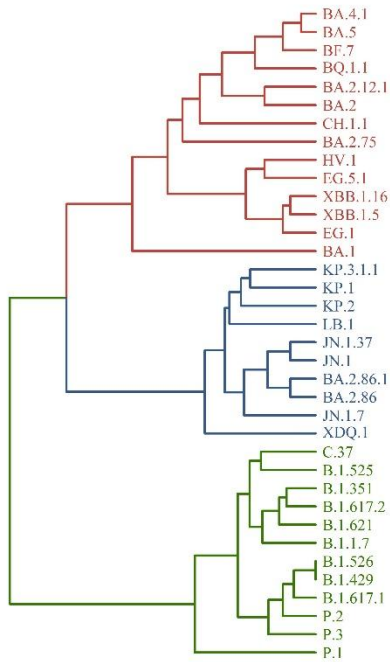
(g) $n=8$, 2-letter

(h) $n=8$, 4-letter

Figure S2 Phylogenetic tree of 36 mutants (total number of mutated sites =128)

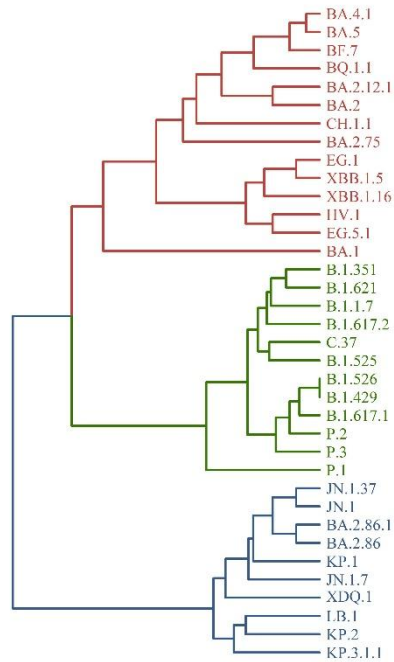


**UPGMA tree for n=7
mutants in 2-letter representation**



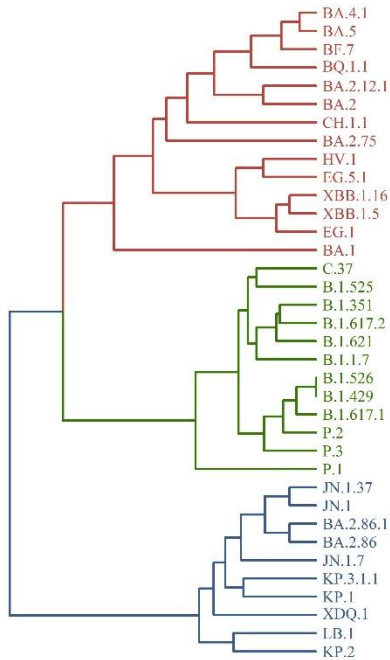
(e) n=7, 2-letter

**UPGMA tree for n=7
mutants in 4-letter representation**



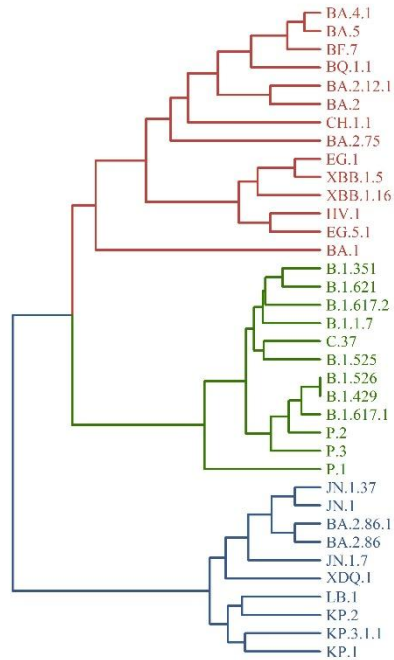
(f) n=7, 4-letter

**UPGMA tree for n=8
mutants in 2-letter representation**



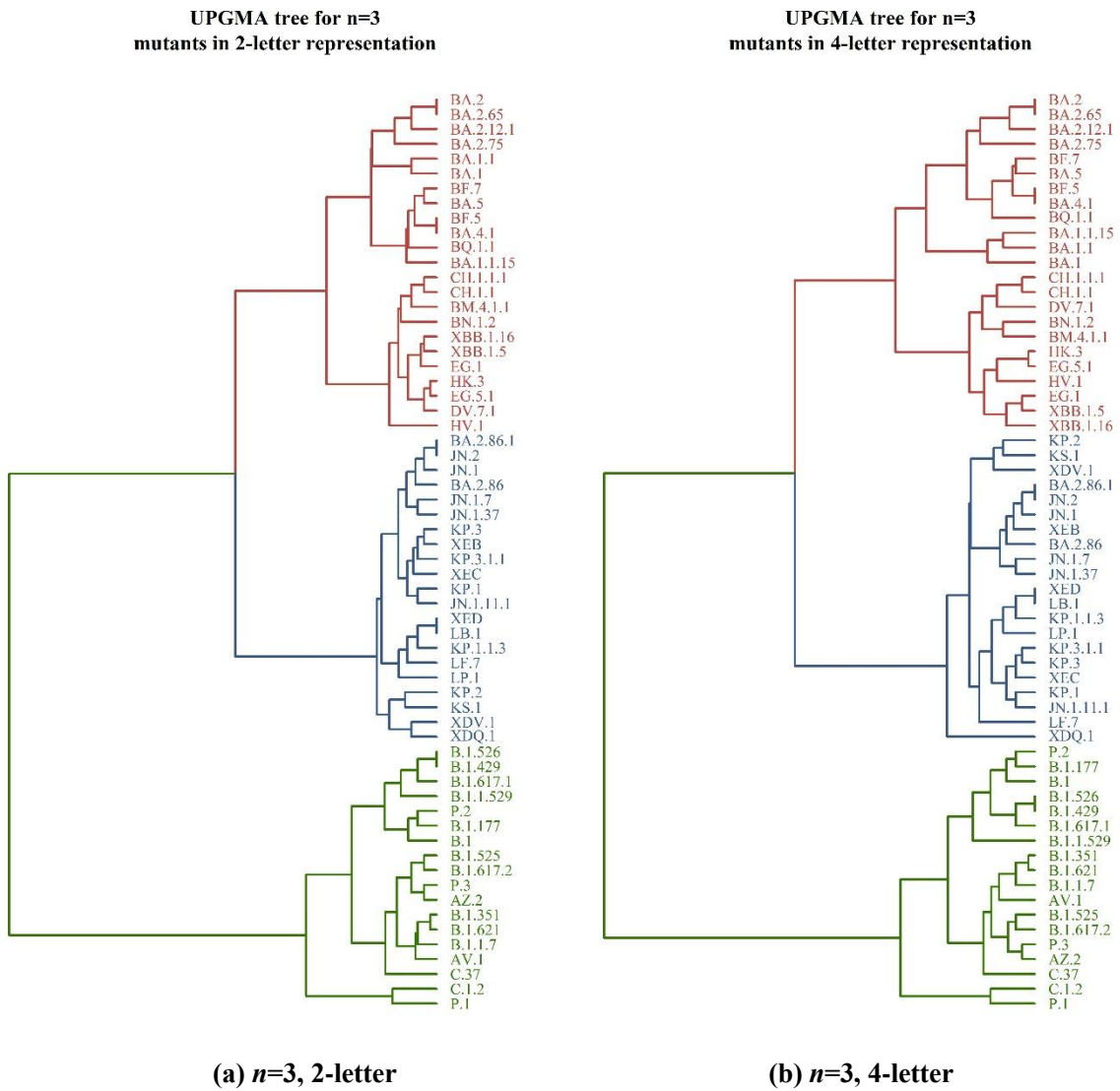
(g) n=8, 2-letter

**UPGMA tree for n=8
mutants in 4-letter representation**

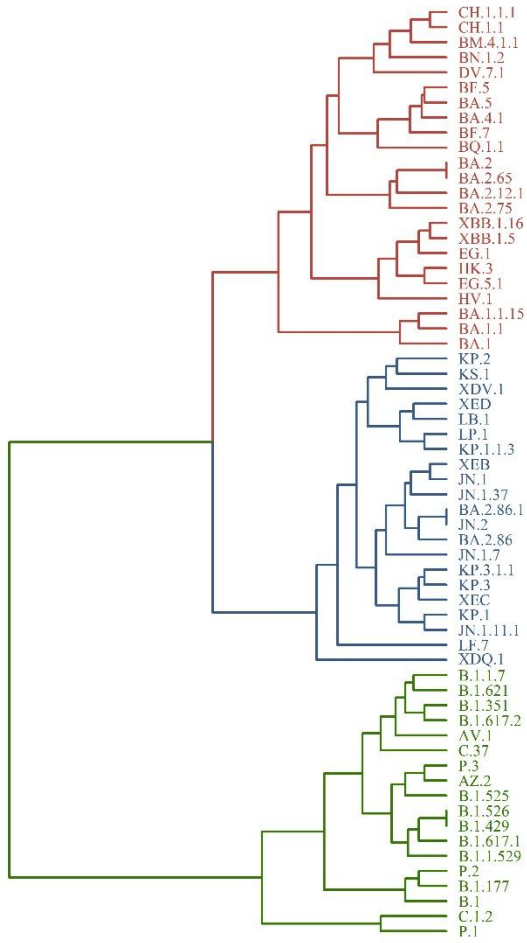


(h) n=8, 4-letter

Figure S3 Phylogenetic tree of 62 mutants (total number of mutated sites =146)

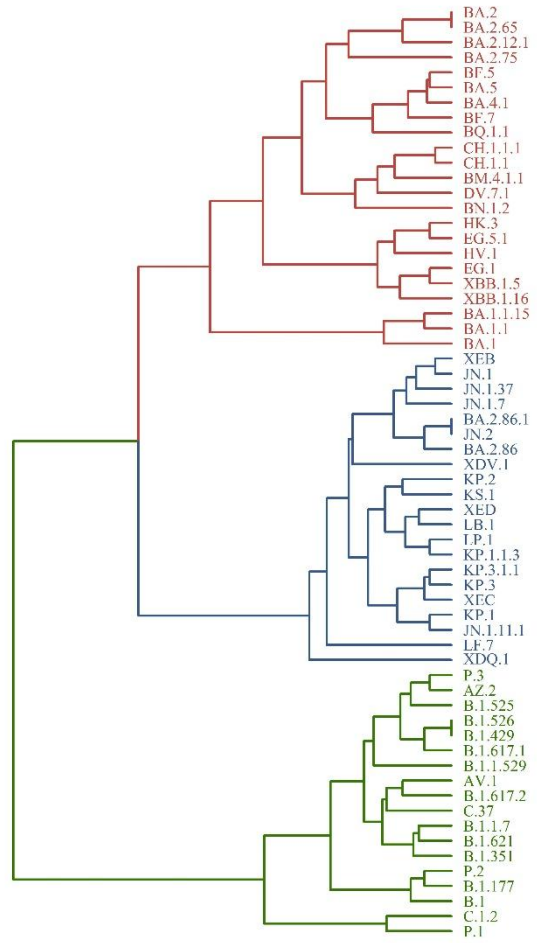


UPGMA tree for $n=5$
mutants in 2-letter representation



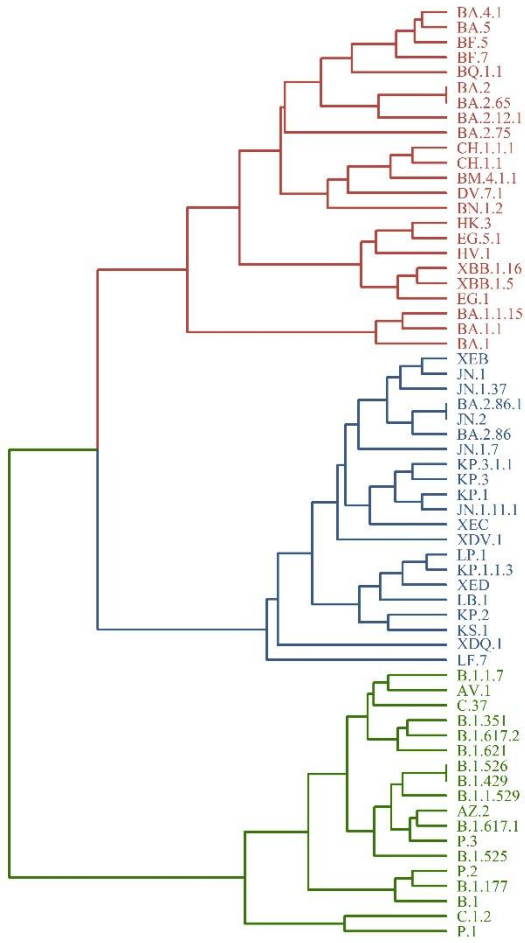
(c) $n=5$, 2-letter

UPGMA tree for $n=5$
mutants in 4-letter representation



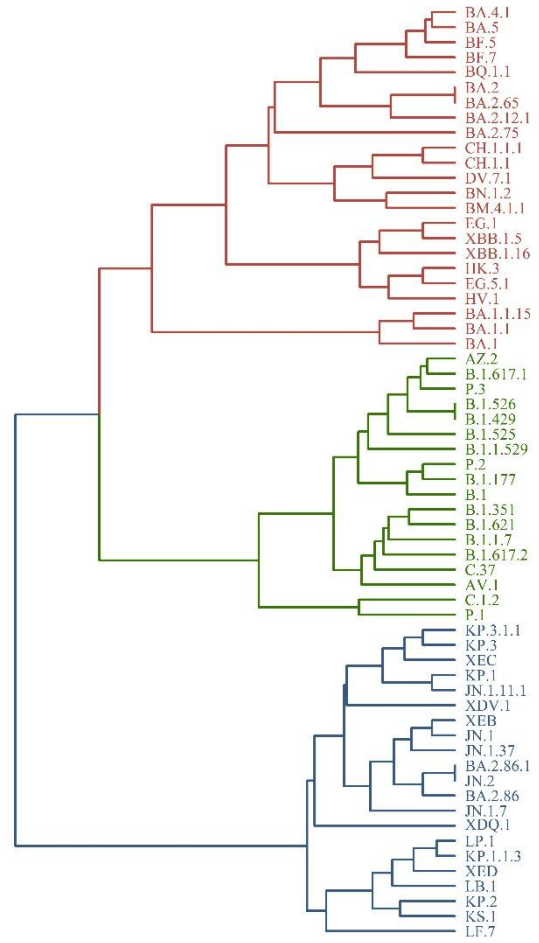
(d) $n=5$, 4-letter

UPGMA tree for $n=7$
mutants in 2-letter representation

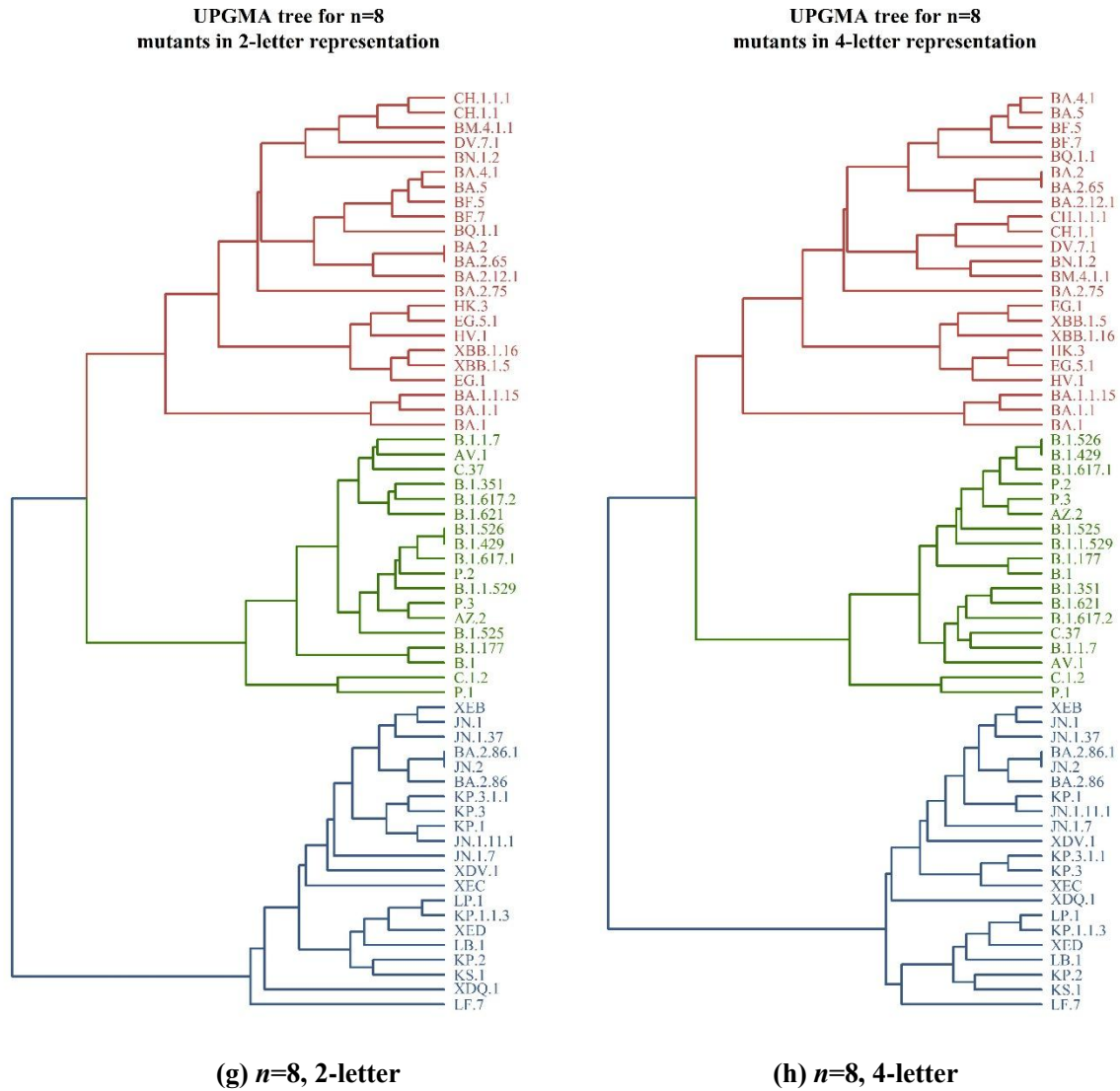


(e) $n=7$, 2-letter

UPGMA tree for $n=7$
mutants in 4-letter representation



(f) $n=7$, 4-letter



Figures S1, S2, and S3 above show the comparison of cladogram structures of phylogenetic trees with different n values and letter representations.

Alternative approach of prediction

Consider the prediction for the new macro-lineage O based solely on the 18 variants of lineage N (Fig. S4A), the prediction for the new macro-lineage P based on the $18 + 23 = 41$ variants of lineages N and O (Fig. S4B), and the prediction for the new macro-lineage Q based on the $18 + 23 + 21 = 62$ variants of lineages N, O, and P (in text Fig. 5). From the data in these figures, we derive the demarcation values x_{dem1} and x_{dem2} presented in Table S4. We observe that the values in Table S4 are essentially identical to those in Table 2.

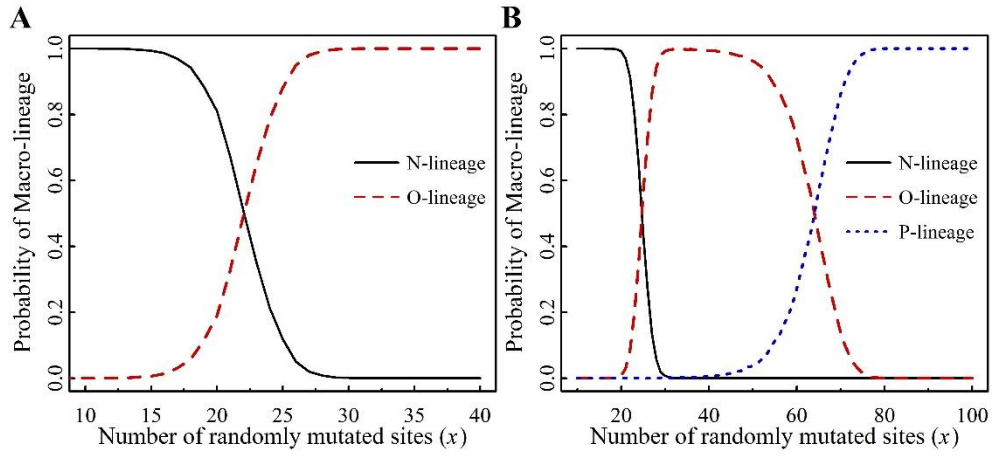


Fig. S4 PML(Probability of Macro-lineage) vs x for 18 variants (in panel A), and 41 variants (in panel B)

Table S4 Demarcation values x_{dem1} and x_{dem2} at three times t_1 and t_2 and t_3

k	a_k	$x_{\text{dem1}}^{(O)}(t_k)$	$x_{\text{dem2}}^{(O)}(t_k)$	$x_{\text{dem1}}^{(P)}(t_k)$	$x_{\text{dem2}}^{(P)}(t_k)$	$x_{\text{dem1}}^{(Q)}(t_k)$	$x_{\text{dem2}}^{(Q)}(t_k)$
1	71	16	28	-	-	-	-
2	117	21	30	43	76	-	-
3	146	21	31	38	63	80	109